Mechatronics Design, Modeling and Preliminary Control of a 5 DOF Upper Limb Active Exoskeleton

Abdelkrim Abane[1,2,3], Mohamed Guiatni[1], Djahid Fekrache[1], Saad Merouche[1], Abdelouahab Otmani[1], Mouloud Tair[2] and Noureddine Ababou[3]

[1]*Control Laboratory, Ecole Militaire Polytechnique, Bordj El Bahri, Algiers, Algeria*

[2]*Hopital Militaire Universitaire Spécialisé, Bouchaoui, Algiers, Algeria*

[3]*Instrumentation Laboratory, Université des Sciences et Technologie Houari Boumedienne, Beb Ezzouar, Algiers, Algeria*

Keywords: Mechatronics Design, Upper Limb Exoskeleton, Robot Modeling, PD Controller.

Abstract: In this paper, we present the mechatronics design, modeling and preliminary control of a new 5 degrees of freedom (DoF) exoskeleton, dedicated for the upper limb rehabilitation. The designed exoskeleton allows the shoulder rotations as well as the elbow movements. It combines the advantages of both parallel and serial mechanisms. It has been designed by considering the main factors in designing a general use robotic force-feedback device and the human upper limb specications. This active device, as a kind of haptic device, provides two ways communication in both position and force, and allows patients to interact with the virtual reality system and practice activities of daily living (ADL) assistance. The kinematic model of the exoskeleton is presented. In order to evaluate the performance of the exoskeleton, a preliminary position and torque controllers have been implemented.

1 INTRODUCTION

Due to the increasing need of physical rehabilitation of the upper extremity, many research groups have proposed robotic devices with the potential to facilitate the rehabilitation process. Many devices for upper limb rehabilitation have already been proposed. These devices have the potential to address this problem as noted by the results of recent research studies. An excellent survey and a state-of-the-art on robotic devices for upper limb rehabilitation is compiled in (Maciejasz et al., 2014) in which more than 200 references and more than 100 devices have been cited and compared in terms of number of degrees of freedom (DOF), actuation, supported movements of the limb (shoulder, elbow, forearm, wrist and fingers), control inputs, type and field of application and their stage of development. A vast majority of these proposed devices are technically advanced and are designed for clinical settings. However, there is still significant need to improve efficiency and reduce cost of home-based devices for therapy and ADLs assistance. The effectiveness of robotic over conventional therapy is arguable and the best therapy strategy is still not clear (Maciejasz et al., 2014) (Jarrassee et al., 2014). The situation may change soon, because more and more devices are being commercialized and more scientific results will be available. It may encourage next groups to propose their own solutions. Developing new devices and improving those already in the market will be easier, when taking advantage from the already existing solutions (Gopura et al., 2011) (Jarrassee et al., 2014) (Chay et al., 2014).

The aim of this work is to propose a new device for the upper limb rehabilitation. The proposed exoskeleton-based devices have a mechanical structure that mirrors the skeletal structure of patients limb. Therefore movement in the particular joint of the device directly produces a movement of the specific joint of the limb. The use of exoskeleton-based rehabilitation allows for independent and concurrent control of particular movement of patients arm in many joints, even if the overall number of assisted movements is higher than six. However, in order to avoid patient injury, we have taken care in our device to adjust lengths of particular segments of the manipulator to the lengths of the segments of the patient arm. Therefore setting-up such device for a particular patient, especially if the device has many segments, may take a significant amount of time.

This paper is organized as follows: Section 2 presents the mechanical design methodology of the

Abane, A., Guiatni, M., Fekrache, D., Merouche, S., Otmani, A., Tair, M. and Ababou, N.
Mechatronics Design, Modeling and Preliminary Control of a 5 DOF Upper Limb Active Exoskeleton.
DOI: 10.5220/0005984203980405
In *Proceedings of the 13th International Conference on Informatics in Control, Automation and Robotics (ICINCO 2016) - Volume 2*, pages 398-405
ISBN: 978-989-758-198-4

new exoskeleton with respect to the design requirement of such a device. Section 3 presents the kinematics of the exoskeleton, forward and reverse kinematic will be computed, the Jaccobian matrix will be derived. These models will be used to develop controller for the exoskeleton. Section 4 develops the control setup and preliminary position and torque control schemes of the 5 DOF exoskeleton based on a Propotional Derivative (PD) and Propotional Integral Derivative (PID) controllers. Finally, we will present some results about the control loops implementation.

2 MECHANICAL DESIGN METHODOLOGY

2.1 Design Considerations

Upper limb rehabilitation devices require movement of shoulder joint and elbow joint for both limbs. The movement of the shoulder and elbow are contributed to the rotation and translation of the wrist. Shoulder is the most complex joint in the human arm i.e., movement of the shoulder joint can be estimated as rotation in single ball-and-socket joint with 3 DOFs. Elbow has a hinge joint which can rotate with 2 DOFs as shown in Fig. 1. The human arm torque requirements during daily activities are presented in table 1.

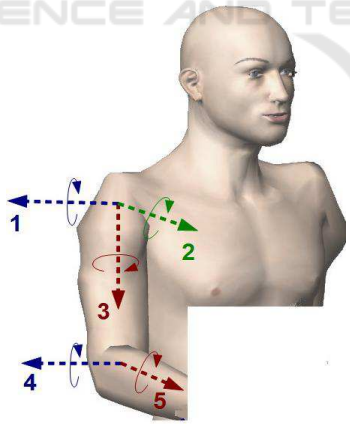

Figure 1: Shoulder and Elbow rotations.

2.2 Hybrid Mechanical Structure Design

When considering the construction of a robotic device, there is a choice between serial and parallel mechanisms (Chen et al., 2014). The key difference between serial mechanisms and parallel mechanisms is in their kinematics structures. Parallel mechanisms

Table 1: Torque Requirement for each rotation (Rosen et al., 2005).

joint	Torque Human max [Nm]	5 % Torque max [Nm]	ADL Torque [Nm]
1	115	5.75	10
2	134	6.5	10
3	60	3	3.1
4	68	3.4	3.8
5	72	3.6	3.8

are composed of, at least, two closed chains that connect a moving platform to a fixed base thus allowing the actuator to be away from the moving platform. For a relatively similar size of the linkages, a serial mechanism presents a larger workspace volume than a parallel mechanism. For parallel mechanism, workspace is compromised by the constraints of all links that connect the end-effector. For serial mechanism, every actuator has to exert enough torque and power to move all distal links and overhead actuators. However, the actuators of a parallel mechanism can be placed on ground to support stronger payload than a serial mechanism does. It can be made so for serial mechanisms, but at the cost of complex transmission mechanisms and this is not always possible for all the links. For parallel mechanism, the geometrical errors are not accumulated, as all the branches are connected to the end-effector. The dimension accuracy of each link must be high so that the position and orientation of the end effector is more accurate than a serial mechanism. For serial mechanism, the geometrical errors are accumulated for each link. Therefore, the end effector will have lower position accuracy. For serial mechanism (Laycock and Day, 2003), each chain increases the total inertia while it decreases the total stiffness. Parallel mechanisms do not exhibit the above problem and have a much higher stiffness (Birglen et al., 2002). The disadvantage over serial mechanisms is that the mechanism's elements can physically interfere. The advantages of both mechanisms are incorporated by combining them in a hybrid configuration (Baser et al., 2006) that includes both parallel and serial linkages. By using hybrid configurations, the stiffness remains relatively high and a large workspace can be achieved.

Our design contains 5 DOF: there is 2 DOF parallel mechanism which insures the abduction/adduction, flexion/extension rotations of the shoulder. This parallel mechanism consists in two legs (chains), each being regarded as a serial manipulator. The first chain constitutes a two-axes serial manipulator and the second chain constitutes a three-axes serial manipulator. These two chains

are coupled through a moving part that supports a third 3 DOF serial chain. The first DOF of this chain ensures the lateral rotation/medial rotation of the shoulder. The fourth and fifth rotations ensure the flexion/extension and the abduction/adduction rotations of the elbow. The design of our device was performed and validated under the SolidWorks software.

2.3 Actuation, Transmission and Reduction

The actuation, the reduction and the transmission are closely coupled and must be designed together. They are selected according to the requirements specified in the last subsection. The type of the incorporated actuators affects the overall weight of the device. In most cases, a good actuator should be compact and light as well as capable of producing the necessary power to deliver necessary forces. There are tradeoffs between power, volume and weight since actuators capable of producing large forces are generally heavier and are larger in size than those actuators capable of smaller forces. The dimensioning procedure of the actuator was performed under MotionWorks plug-in of Solidworks, by applying dynamic forces on device end-effector and then obtaining the required actuator torques. We select brushed Maxon DC motors with a low inertia and low friction, which are suitable for this kind of devices. Maxon RE40 is used for the abduction/adduction, flexion/extension rotations of the shoulder and RE25 for the flexion/extension and the abduction/adduction rotations of the elbow and the lateral rotation/medial rotation of the shoulder.

In order to provide the highest amount of fidelity, direct drive (absence of transmission of reduction) is likely to be the best solution. However, this solution does not provide adequate forces/torques needed for our application, which we saw earlier is critical. Among the other transmission and reduction techniques such as the use of linkages, cables, steel belts, shafts plus gears, this last one gives the worst case (Hayward, 1995) since it causes high backlash and high back-drive friction due to the gear gaps and gear friction. Back-drive friction and backlash can be reduced by using cable driven transmission systems. Therefore, cable driven transmission technique (capstan) was used in our design.

A solution consists of using a combined reduction (Planetary gear/capstan) in order to amplify the torques developed by the actuators. We use planetary gears reduction because it has fewer backlashes and less friction, especially when the reduction ratio is small (the reduction ratio are 4 for RE40 actuators and 19 for the RE25 actuators in this case). We have designed capstan reduction mechanisms with a ratio of 20 for the abduction/adduction and flexion/extension rotations of the shoulder and 10 for the lateral rotation/medial rotation of the shoulder and the flexion/extension and the abduction/adduction rotations of the elbow. The resulting reduction ratios and the maximal torque that could be generated for each axis are presented in Table 2. This solution is able to provide additional torque for gravity and friction compensation.

Table 2: Reduction ratio and maximal torque for each joint.

J	Motor	Total Ratio	Resol.	Max Torque $(N.m)$
1	RE40	80	0.009°	14.5
2	RE40	80	0.009°	14.5
3	RE25	190	0.004°	5.6
4	RE25	12	0.06°	0.83
5	RE25	190	0.004°	5.6

As it was presented previousely, the exoskeleton should include low inertia, no backlash, light weight and negligible friction (Laycock and Day, 2003). Therefore, a compromise has to be reached between the various design goals. Obtaining negligible friction can be a problem, particularly when high stiffness is required. High stiffness implies a stiff mechanical interface which needs to be constructed from metal which increase the friction and the overall weight of the device. This provides a conflict between obtaining high stiffness while keeping low friction (Baser et al., 2006)(Laycock and Day, 2003). So that, the materials used to construct such devices need to be considered with additional costs. In our design:

- Aluminum was used in order to minimize the deflection due to the stiffness of the linkages.
- Cable driven transmission technique was used in order to overcome backlash deflection.
- Stainless steel ball bearings and high precision manufacturing methods were used in order to overcome joint deflections.

The Computer Aided Design (CAD) model of the exoskeleton is shown in Figure 2 and table 3.

2.4 Stress and Deflection Analysis

After the completion of the preliminary mechanical design procedure, links shape and thickness must be optimized to satisfy the design requirements mentioned before, such as the reduction of the inertia of the device and the maximization of the stiffness. For this structure, the links stress analysis is carried out using COSMOSXpress plug-in of Solidworks. Static

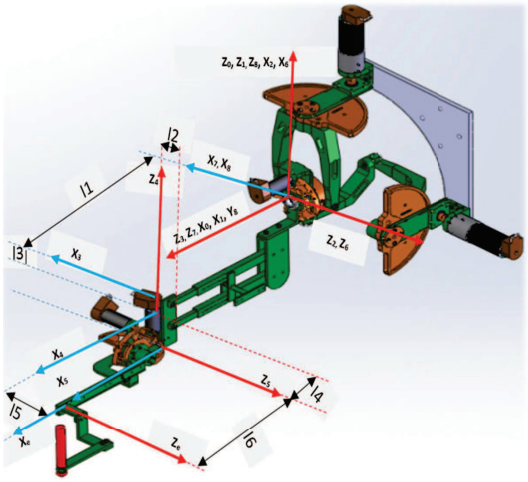

Figure 2: CAD Model of the designed exoskeleton.

Table 3: Parts designation for the CAD model.

$N°$	Designation	$N°$	Designation
01	Motor 1 (RE40)	13	Body 2
02	Gear (GP42)	14	Capstan 4 (12:1)
03	Capstan 1 (20:1) (20:1)	15	Adjustable link
04	Body 1	16	Body 4
05	Motor 3 (RE25)	17	Capstan 3 (10:1)
06	Encoder 3 (HEDS 5540)	18	Body 3
07	Encoder 4 (HEDS 5540)	19	Capstan 2 (20:1)
08	Motor 4 (RE25)	20	Encoder 2 (HEDS 5540)
09	Encoder 5 (HEDS 5540)	21	Motor 2 (RE40)
10	Motor 5 (RE25)	22	Gear (GP42)
11	Capstan 5 (10:1)	23	Fixed base
12	End-effector	24	Encoder 1 (HEDS 5540)

analysis of the mechanical design would be sufficient because the device will be used with low speeds. The links shape and weights are computed for aluminum with a Young modulus of 69000 MPa and a mass density of 2700 kg/m^3 as construction material. This material is used because of its high yield strength over weight ratio. According to the analysis results, the shape and the thickness of the links should be modified in iterations. The weight values of the motors, reductors and links starting from the tool tip and moving to the base of the robot are used to determine the static load on the robot links.

In Figure 3, an example of deformation and distribution of von-Mises stresses are illustrated for two links of the manipulator. Contour diagram and maximum stress points are shown in the figures. Legend on the right side of the figure shows the distribution of contour diagram. Legend on the right hand side of the figure shows the distribution of contour diagram. In this analysis, deformation in the translational movement direction is studied under static loading of 50 N, which corresponds to the maximum force that shall be applied during MIS procedures. Naturally, maximum deflection occurs at the end of the links. The maximum and minimum deformation points are shown in the figure. It has been observed that the link 1 and 3 (parts 06 and 17 in table 3) are the most critical links since they are exposed to maximum stress in any condition. The shape and thickness of the links are optimized according to the maximum deflection values obtained from the analysis. Figure 4 represents the manufactured exoskeleton.

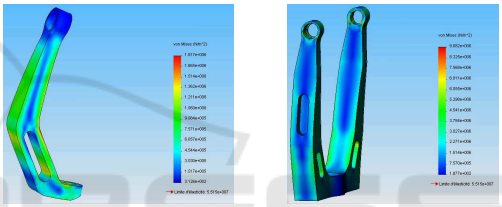

Figure 3: Von-Mises Stress analysis of links 1 (left) and 3 (right).

Figure 4: Final prototype of the exoskeleton.

3 EXOSKELETON MODELING

3.1 Kinematic Modeling

Figure 5 shows the position of the frames attach-

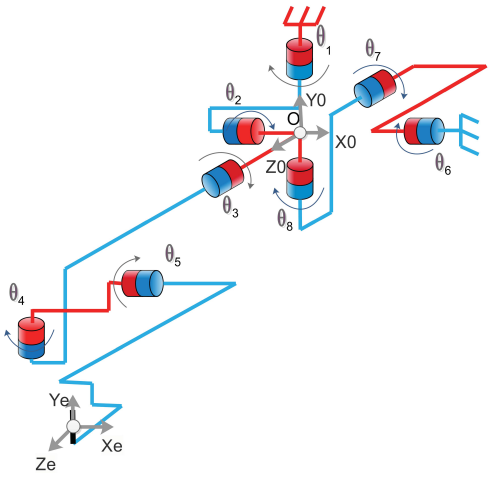

Figure 5: Kinematics of the exoskeleton.

ments. All the frames intersect at one point named 'O' situated at the center of the moving platform that connects the two parallel chains to each other, thus simplifies the kinematics modeling. For each chain, the kinematics model is obtained by using the modified method of Denavit and Hartenberg (Khalil and Dombre, 1999), where ${}^{i-1}R_i$ represents the rotation matrix from the frame $F_{i-1}(x_{i-1}, y_{i-1}, z_{i-1})$ to the frame $F_i(x_i, y_i, z_i)$.

Kinematics parameters are defined in tables 4 and 5, where α_j represents the joint offsets, r_j and L_j the link lengths and θ_j the joint variables. The moving platform is a body of both Chain 1 and Chain 2. In Chain 1, it is referenced by the frame F_2 and in chain 2 by F_6. So that, the kinematics constraints representing the closure condition of the parallel structure formed by Chain 1 and Chain 2 are then:

$$\theta_2 = \arctan(\tan(\theta_6)/C_1) \tag{1}$$

Table 4: DHM kinematics parameters of Chain 1.

j	α_j	L_j	θ_j	r_j
1	$\pi/2$	0	θ_1	0
2	$\pi/2$	0	θ_2	0
3	$\pi/2$	0	θ_3	L_0
4	$-\pi/2$	$-L_1$	θ_4	$-L_2$
5	$-\pi/2$	L_3	θ_5	L_4
6	$-\pi/2$	0	0	L_5

Table 5: DHM kinematics parameters of Chain 2.

j	α_j	d_j	θ_j	r_j
6	$-\pi/2$	0	θ_6	0
7	$-\pi/2$	0	θ_7	0
8	$-\pi/2$	0	θ_8	0

and:

$$\begin{cases} \theta_7 = \arctan 2\left((S_1 S_2), \pm\sqrt{1-(S_1 S_2)^2}\right) \\ \theta_6 = \arctan 2\left((C_1 S_2/C_7), (C_2/C_7)\right) \\ \theta_8 = \arctan 2\left((S_1 C_2/C_7), (C_1/C_7)\right) \end{cases} \tag{2}$$

Where Ci and Si stand for $\cos(\theta_i)$ and $\sin(\theta_i)$, respectively.

The angular positions of the passive joints θ_2, θ_7 and θ_8 are computed based on the angular positions of the active joints θ_1 and θ_4. Expressions (1) and (2) are not defined for $\theta_1 = \pm\frac{\pi}{2}$ and $\theta_2 = \pm\frac{\pi}{2}$. Fortunately, all these configurations are outside the reachable workspace.

The orientation and position of the end-effector is determined by taking the joint angles of the linkages and using the forward kinematics calculation as follows:

$${}^0T_e = {}^0T_1\,{}^1T_2\,{}^2T_3\,{}^3T_4\,{}^4T_5\,{}^5T_e$$

$${}^0T_e = \begin{pmatrix} s_x & n_x & a_x & {}^0p_x \\ S_y & n_y & a_y & {}^0p_y \\ s_z & n_z & a_z & {}^0p_z \\ 0 & 0 & 0 & 1 \end{pmatrix}$$

Thus, the kinematic model of the exoskeleyon is defined as follows:

$$\begin{cases} {}^0p_x = S_1(-S_2C_3(L_2+l_5S_5)+S_2S_3(-L_1+L_3S_4 \\ \quad +L_4C_4+L_5C_5)+C_1((L_5C_5S_4+L_3S_4 \\ \quad +L_4C_4-L_1)C_3+S_3(L_5S_5+L_2))_4+l_0)) \\ \quad -C_2(L_5C_5C_4+l_3C_4-L_4S_4+L0)) \\ {}^0p_y = C_2(S_3(L_5C_5S_4+L_3S_4+ \\ \quad L_4C_4-L_1)-C_3(L_5S_5+L_2)) \\ \quad +S_2((L_3+L_5C_5)C_4-L_4S_4+L_0) \\ {}^0p_z = S_1(S_2C_3(L_2+L_5S_5)-S_2S_3 \\ \quad (-L_1+L_3S_4+L_4C_4+L_5C_5) \\ \quad +S_1((L_5C_5S_4+L_3S_4+ \\ \quad L_4C_4-L_1)C_3+C_3(L_5S_5+L2)) \\ \quad +C_2(L_5C_5C_4+L_3C_4-L_4S_4+L_0)) \end{cases} \tag{3}$$

where ${}^0p_x$, ${}^0p_y$, ${}^0p_z$ represents the position of the end-effector defined in the frame ${}^0F$ and (s, n, a) its orientation. We use the Euler angles (α,β ,γ) in order to define this orientation as follows:

$$\begin{cases} \beta = \arctan 2\left(-s_z, \sqrt{{s_x}^2+{s_y}^2}\right) \\ \alpha = \arctan 2\left(s_y/\cos(\beta), s_x/\cos(\beta)\right) \\ \gamma = \arctan 2\left(n_z/\cos(\beta), n_y/\cos(\beta)\right) \end{cases} \tag{4}$$

where :

- α defines the rotation around the Z_0 axis.
- β defines the rotation around the Y_0 axis.
- γ defines the rotation around the X_0 axis.

and

$$\begin{cases} s_x = C_4(S_1S_2S_3 + C_1C_3) + S_1C_2S_4 \\ s_y = C_2S_3C_4 - S_2S_4 \\ s_z = C_4(C_1S_2S_3 - S_1C_3) - C_1C_2S_4 \\ n_y = S_4(C_2S_3S_5 + C_4S_2) + C_2C_3C_5 \\ n_z = S_5(S_4(S_1C_3 - C_1S_2S_3) + S_1C_2C_4) + C_2C_3C_5 \end{cases} \quad (5)$$

The workspace of the exoskeleton is presented in Table 6.

Table 6: Designed exoskeleton vs human arm workspace comparison.

j	Joint	Human arm	Exoskeleton
1	Adduction /abduction (shoulder)	-45/180°	-45/100°
2	Extension /flexion (shoulder)	-50/180°	-45/100°
3	External /internal rotation	-80/90°	-70/70°
4	Adduction /abduction (Elbow)	0/200°	0/140°
5	Extension /flexion (Elbow)	0/145°	0/140°

3.2 Jaccobian Matrix

The Jacobian matrix J is one of the most important quantities in the analysis and control of robot motion. It arises in virtually every aspect of robotic manipulation: in the planning and execution of smooth trajectories, the execution of coordinated anthropomorphic motion, in the derivation of the dynamic equations of motion, and in the transformation of forces and torques from the end-effector to the manipulator joints and in the determination of singular configurations.

The resulting Jaccobian matrix of the exoskeleton is defined as follows:

$$J = \begin{pmatrix} J_{11} & J_{12} & J_{13} & J_{14} & 0 \\ J_{21} & J_{22} & J_{23} & -L_4S_5 & -L_5 \\ J_{31} & J_{32} & J_{33} & -C_5L_4 & 0 \\ J_{41} & -C_4C_3 & -S_4 & 0 & 1 \\ J_{51} & J_{52} & S_5C_4 & C_5 & 0 \\ J_{61} & J_{62} & C_4C_5 & -S_5 & 0 \end{pmatrix} \quad (6)$$

where,

$$\begin{cases} J_{11} = C_1(C_3(-(C_5L_6 + L_4)S_4 - L_5C_4 + L_2) \\ \quad -S_3(S_5L_6 + L_3)) - S_1(S_2(-S_3(-S_3 \\ \quad (-(C_5L_6 + L_4)S_4 - L_5C_4 + L_2) \\ \quad -C_3(S_5L_6 + L_3)) \\ \quad +C_2(C_4(C_5L_6 + L_4) - S_4L_5 + L_1)) \\ J_{12} = (-S_5S_4C_3 + C_5S_3)L_5 - C_3L_2S_4 \\ \quad +S_3(C_4L_0 - L_1S_4 + L_3) \\ J_{13} = S_5C_4L_5 + C_4L_2 \\ J_{14} = C_5L_5 + L_3 \\ J_{21} = ((L_3S_3C_2 - L_4S_2)C_4 \\ \quad +(-L_4S_3C_2 - S_2L_3)S_4 \\ \quad +L_1S_2 + S_3C_2L_0)C_5 + (-C_2 \\ \quad (-L_2S_3 + L_1C_3)C_4 + (-C_3C_2L_0 - L_2S_2) \\ \quad S_4 + L_4C_3C_2)S_5 + L_5(C_4S_3C_2 - S_2S_4) \\ J_{22} = ((L_2C_3 + L_1S_3)C_4 + S_3L_0S_4 \\ \quad -L_4S_3)S_5 + L_5C_4C_3 \\ \quad +(L_3C_3C_4 - L_4C_3S_4 + C_3L_0)C_5 \\ J_{23} = (L_4C_4 + L_3S_4 - L_1)C_5 \\ \quad +L_2S_4S_5 + L_5S_4 \\ J_{31} = ((L_4S_2 - L_3S_3C_2)C_4 + (L_4S_3C_2 + S_2L_3)S_4 \\ \quad -S_3C_2L_0 - L_1S_2)S_5 - C_5(C_2(-L_2S_3 + L_1 \\ \quad C_3)C_4 + (L_2S_2 + C_3C_2L_0)S_4 - L_4C_3C_2) \\ J_{32} = (-(L_2C_3 + L_1S_3) \\ \quad C_4 - S_3L_0S_4 + L_4S_3) \\ \quad -C_5(-L_3C_3C_4 + L_4C_3S_4 - C_3L_0)S_5 \\ J_{33} = (-L_4C_4 - L_3S_4 + L_1)S_5 + C_5L_2S_4 \\ J_{41} = S_2S_4 - C_4S_3C_2 \\ J_{51} = (-S_4S_3C_2 - C_4S_2)S_5 - C_5C_3C_2 \\ J_{52} = -S_5S_4C_3 + C_5S_3 \\ J_{61} = (-S_4S_3C_2 - C_4S_2)C_5 + S_5C_3C_2 \\ J_{62} = -S_4C_3C_5 - S_5S_3 \end{cases} \quad (7)$$

4 ELECTRONICS INTERFACE AND PRELIMINARY CONTROL LOOP DESIGN

4.1 Position and Current Sensing

The angular positions of the five active joints are measured thanks to five incremental encoders type HEDS 5540 from Maxon. These encoders are placed in the rear of the motors and provide 500 pulsations per revolution of the motor axis. Thus, the position measurement resolution is computed by taking into account, the reduction ratio $((360/500)/N$, while N is the reduction ratio). Table 2 presents the angular position resolution of each joint. Current sensors type LTS 15-NP are also integrated in order to measure the actuator's current. The measured current is used in order to estimate the actuator's torque.

4.2 Electronics Interface

The control setup consists in a dSPACE DS1103 Control Board which is a versatile and powerful real-time measurement and control board. The power stage is designed based on two OPA541 and three OPA548 operational power amplifiers from Burr-Brown which are able to provide a current about 10 for RE40 motors and 3A for RE25 motors respectively (Fig. 6).

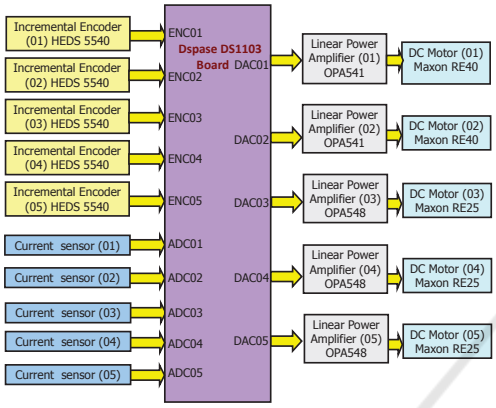

Figure 6: Overview of the electronics interface.

4.3 Preliminary Control Loop Design

In order to assess the model and to evaluate the performances of the assembled exoskeleton, basic position and torque control loops are implemented. We used proportional-derivative (PD) and proportional-derivative-intergral (PID) controllers respectively for each joint of the exoskeleton (see Fig.7 for position control and Fig.8 for torque control). In Fig.8, constants K_i $(i = 1,...5)$ represent the torque constants of the actuators.

These preliminary controllers have been implemented successfully. Figure 9 presents an example of the obtained results for sinusoidal position tracking while Fig. 10 presents an example of the obtained results for square torque tracking. These results show that the PD controller allows improving the time response of the system and eliminating the static error in the position control loop in a stable way. Similar remarks are recorded for the torque controller. So that, and since the first instant, the resulting trajectory converges faster to the desired one. These results show the good tracking capability of the developped exoskeleton.

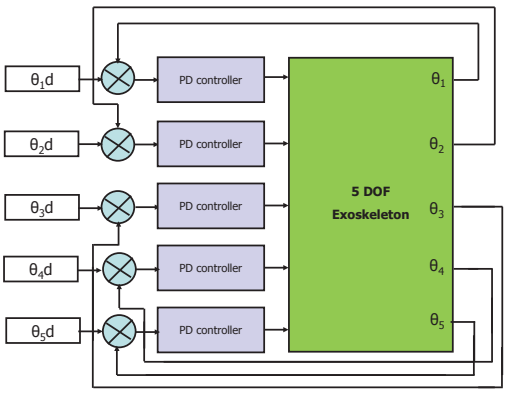

Figure 7: Preliminary position control scheme.

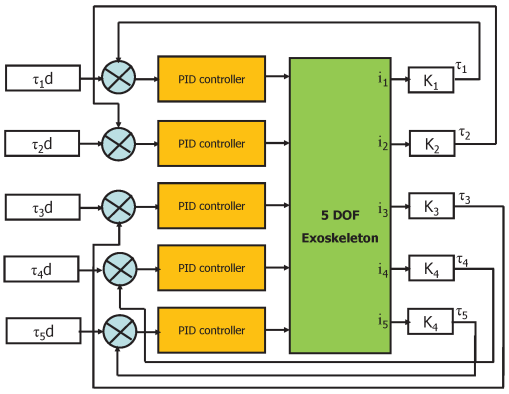

Figure 8: Preliminary torque control scheme.

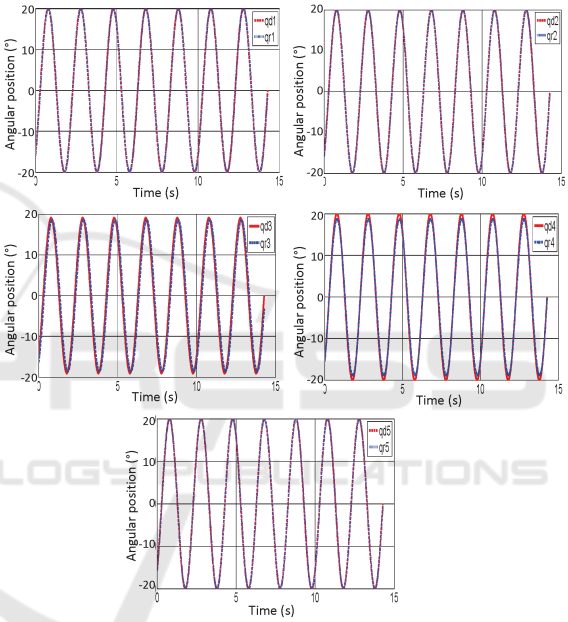

Figure 9: Articular position control example.

5 CONCLUSION

A new exoskeleton has been designed and realized for the upper limb rehabilitation objective. This new device takes benefits from both the advantages of serial

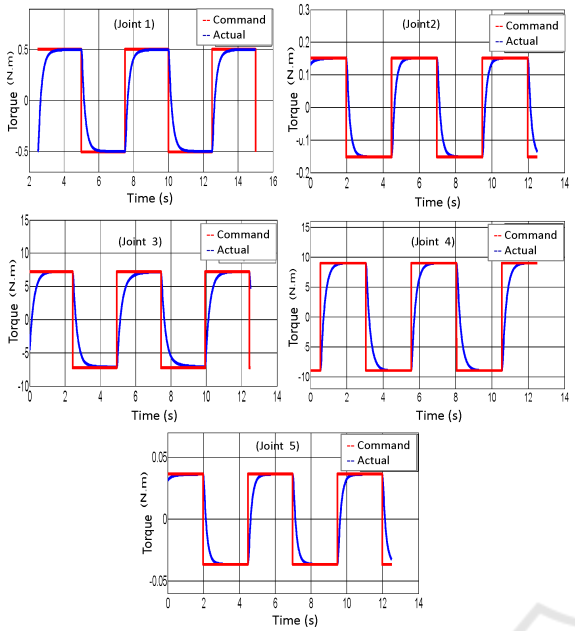

Figure 10: Articular torque control example.

mechanisms and parallel mechanisms. It allows moving the shoulder joint around three axes and the elbow around two axes. Kinematics of the exoskeleton has been computed, and its capabilities have been determined and compared to the requirements. Preliminary position and torque control loops have been implemented in order to evaluate the basic performance of the device in term of position and torque tracking. Future works will concern a bandwidth analysis, model based control, admittance control, and clinical evaluation of the exoskeleton.

REFERENCES

Baser, O., Konukseven, E. I., and Koku, B. (2006). 7 dof haptic device design. In *EuroHaptics 2006*, pages 507–512.

Birglen, L., Gosselin, C., and Pouliot, N. (2002). Shade, a new 3-dof haptic device. *IEEE Transactions on Robotics and Automation*, 18(2):166–175.

Chay, K.-H., Lee, J.-V., Chuah, Y.-D., and Chong, Y.-Z. (2014). Upper extremity robotics exoskeleton: Application, structure and actuation. *International journal of Biomedical Engineering and Science*, 1(1):35–45.

Chen, Y., Li, G., Zhu, Y., Zhao, J., and Cai, H. (2014). Design of a 6-dof upper limb rehabilitation exoskeleton with parallel actuated joints. *Biomed Mater Eng.*, 24(6):2527–2535.

Gopura, R. C., Kiguchi, K., and Bandara, S. V. (2011). A brief review on upper extremity robotic exoskeleton systems. In *6th IEEE International Conference on Industrial and Information Systems*, pages 346–351.

Hayward, V. (1995). Toward a seven axis haptic device. In *International Conference on Intelligent Robots and Systems*, pages 31–33, Washington, DC, USA. IEEE Computer Society.

Jarrassee, N., Proietti, T., Crocher, V., Robertson, J., Sahbani, A., Morel, G., and Roby-Brami, A. (2014). Robotic exoskeletons: A perspective for the rehabilitation of arm coordination in stroke patients. *Frontiers in Human Neuroscience*, 8(947).

Khalil, W. and Dombre, E. (1999). *Modélisation, identification et commande des robots*. Collection robotique.

Laycock, S. D. and Day, A. M. (2003). Recent developments and applications of haptic devices. *Computer Graphics, Blackwell Publishing Ltd*, 22(2):117–132.

Maciejasz, P., Eschweiler, J., Gerlach-Hahn, K., Jansen-Troy, A., and Leonhardt, S. (2014). A survey on robotic devices for upper limb rehabilitation. *Journal of NeuroEngineering and Rehabilitation*, 11(3):1–29.

Rosen, J., Perry, J. C., Manning, N., Burns, S., and Hannaford, B. (2005). The human arm kinematics and dynamics during daily activities-toward a 7 dof upper limb powered exoskeleton. In *Advanced Robotics, 2005. ICAR'05. Proceedings., 12th International Conference on*, pages 532–539. IEEE.